Published in IET Electrical Systems in Transportation
Received on 28th March 2013
Revised on 4th August 2013
Accepted on 17th September 2013
doi: 10.1049/iet-est.2013.0016

ISSN 2042-9738

Optimal design of line level control resonant converters in plug-in hybrid electric vehicle battery chargers

Sideng Hu[1], Junjun Deng[1,2], Chris Mi[1], Mengyang Zhang[3]

[1]*University of Michigan-Dearborn, Dearborn, MI 48128, USA*
[2]*Northwestern Polytechnical University, Xi'an 710072, People's Republic of China*
[3]*Chrysler Group, LLC, Auburn Hills, MI, USA*
E-mail: mi3032@gmail.com

Abstract: The series–parallel resonant converter (also called line level control (LLC) resonant converter) is one of the most suitable topologies for dc–dc power supply. This study introduces the LLC resonant converter into the on-board battery chargers for the plug-in hybrid electric vehicle (PHEV) applications. Different from the previous literature which has focused on the wide operation range and hold-up time requirement in the LLC design, this study is mainly focused on battery load characteristics and its impact on the charger design. First, to guarantee high efficiency in the light-load condition in the constant voltage charging stage, the optimum LLC switching frequency range is derived. Second, considering the constant current charging function in the battery charger, the impact of peak load current on the LLC converter is discussed. The boundary between zero-voltage switching (ZVS) and zero-current switching (ZCS) in the constant current charging application is analysed. The trade-off among the minimum load voltage, maximum charge current and resonant capacitor is studied in detail. Finally, the optimal design method for the LLC resonant converter used in the PHEV battery charger is proposed. The proposed methods are validated through experiments on a 400 V/6 kW PHEV charger system with 97% efficiency.

1 Introduction

High efficiency, small size and high reliability are the basic requirements for an on-board battery charger in plug-in hybrid electric vehicle (PHEV) and electric vehicle (EV) applications. The size, cost and mechanical packaging are well discussed from practical aspect in [1]. A comprehensive topological survey of the currently available charging solutions is presented in [2]. The conventional pulse width modulation (PWM) technology with hard-switching suffered from severe switching losses and electromagnetic interference (EMI) issues. Resonant converters were reported in many papers recently because of their simple structure, high efficiency and low EMI [3, 4]. Among many resonant converters, the full bridge series–parallel resonant converter (SPRC, also called line level control (LLC) resonant converter) is more suitable than other resonant converters for PHEV charger applications [3, 4]. Compared with series resonant converters, the LLC converter can work in both buck and boost mode [3]. The integration of the inductors into a transformer makes the volume of a LLC converter smaller than a parallel resonant converter. However, the load-dependent properties of LLC resonant converters make the design more complicated. Researchers have mainly focused on the design method based on the first harmonic approximation (FHA) method [3–6]. Choi [4] and Yang *et al.* [5] analysed the dead-time optimal method with FHA. Beiranvand and Rashidia [7] discussed the FHA method in the wide output range LLC converter design. Hu and Qiu [8] presented a switch-controlled capacitor modulated LLC converter with a constant switching frequency for multiphase paralleling. This can help multiply the load capacity. Tomokazu and Mizutani [9] added an anti-resonant circuit into the LLC converter to improve the voltage conversion ratio in the dc voltage step-down area.

In the previous literature, the load characteristics is usually assumed to be passive, such as a resistor, in the theoretical analysis and experiments for the optimisation. The load characteristics and its impact are not well researched. For a battery charger, however, the optimal design requirements are quite different [10, 11].

First, more non-linear characteristic exists in the design for a resonant converter with a battery load. Table 1 shows the comparison of a PWM converter and a resonant converter with a passive load and a battery load.

For a dc power supply is connected with a passive load, the load voltage is largely determined by the load current. When the load is a battery, the load voltage is related to the battery state-of-charge (SOC) during the charging process. The charger output voltage is clamped by the battery voltage and is less dependent on the load current. From the converter topology aspect, the conventional PWM voltage source converters are largely unaffected by the load current.

Table 1 Comparison of the converters with a passive load and a battery load

	PWM converter with passive load	Resonant converter with passive load	PWM converter with battery load	Resonant converter with battery load
switching current and load current	proportional	independent	proportional	independent
load voltage and load current.	proportional	proportional	independent	independent
design challenge	easy	normal	normal	difficult

Consequently, the switch current is proportional to the load current. Meanwhile, the conduction loss turned to be small at light load, leading to good light-load efficiency. These properties, however, are not exhibited in the resonant converters. In a resonant converter, the switch current is equal to the resonant tank current i_1 and is less dependent on load current.

From Table 1, we can find that the design for a resonant converter with a battery load is more complicated than other applications. Both of the non-linear characteristics in the resonant tank and the battery need to be considered.

Second, the load voltage varies significantly in the whole charging process. For a single cell lithium-ion battery (4.2 V/cell), the voltage increment could be more than 0.6 V per cell as SOC reaches the full level from zero. That means at least 60 V increment for a whole battery package applied for a 400 V PHEV drive system. As a result, the system should be capable to work in a wide operation range.

Third, the charge process for a lithium-ion battery contains two stages: a constant current (CC) charging stage and a constant voltage (CV) charging stage. The design requirements are not the same in the two stages. For the benefits of saving charging time, in the CC charging stage, a large charge current is preferred. While in the CV charging stage, the charge current is much smaller than in the CC stage. Hence, the light-load efficiency and overcharging issues are more important. Most of previous researches focused on charging currents, battery performance and overcharging problems in each charging process. Dickinson and Gill [12] analysed the issues and benefits with fast charging for the industrial batteries, and Li *et al*. [13] explored the charging method for lead-acid batteries of EV s based on the battery model; however, the optimum design for both charging stages on a battery charger needs more investigation.

Based on the above analysis, the design of a PHEV battery charger based on LLC converters is more challenging compared with the design with a regular passive load. In this paper, the operation frequency range for the battery load is derived and analysed in Section 3 to achieve high efficiency in the CV charging stage. Section 4 focused on the impact of battery load on the CC charging stage of the LLC converters. The optimal design procedure is presented in Section 5 and the experimental results are presented in Section 6. All of the analyses are validated through experiments on a 400 V/6 kW PHEV on-board battery charger.

2 Operation principle of LLC resonant converters with a battery load

A typical schematic of a full bridge LLC multi-resonant dc–dc converter is shown in Fig. 1, where C_r is the resonant capacitor, L_m is the magnetising inductance and L_r is the leakage inductance in the primary side. The advantages of LLC resonant converters include primary-side zero-voltage switching (ZVS), secondary-side zero-current switching (ZCS), integrated magnetic component and buck/boost operation capability [5].

As shown in Fig. 1, different from a conventional PWM converter, the output of a resonant converter is controlled indirectly through the resonant tank [14]. The tank exchanges a large amount of energy with the source and load. The input voltage V_{tank} is a symmetrical square waveform with a magnitude of V_{in}, frequency f_s and duty ratio of 50%. When f_s is close to f_r, the resonant tank primarily responds to the fundamental (f_s) component V_{s1} of V_{tank} and the harmonics voltage at frequencies (nf_s) of V_{tank} have negligible response. Hence, the input voltage waveform $V_{tank}(t)$ can be well approximated by its fundamental component V_{s1}, which is in phase with the square wave V_{tank}(t)

$$V_{s1} = \frac{4V_{in}}{\pi}\sin(\omega_s t) \tag{1}$$

ZVS occurs when the impendence of the resonant tank is inductive, that is, tank current $i_1(t)$ lags voltage V_{s1}, while ZCS occurs when the impendence of resonant tank is capacitive, that is, tank current leads voltage V_{s1}.

Different from conventional resonant converters, the LLC resonant circuit is a kind of multi-resonance circuit. There are two resonant frequencies that can be expressed as

$$f_{r1} = \frac{1}{2\pi\sqrt{L_r C_r}} \tag{2}$$

$$f_{r2} = \frac{1}{2\pi\sqrt{(L_r + L_m)C_r}} \tag{3}$$

The dc gain of output voltage in a LLC converter is not only related to f_s but also related to the load situation [15]. The frequency response of the output voltage under load variations is shown in Fig. 2. The load quality factor Q is defined by $\sqrt{L_r/C_r}/R_{Load}$.

Soft-switching is one of the advantages of a LLC resonant converter because of its effect on the reduction of switching loss and EMI. Various forms of soft-switching such as ZVS

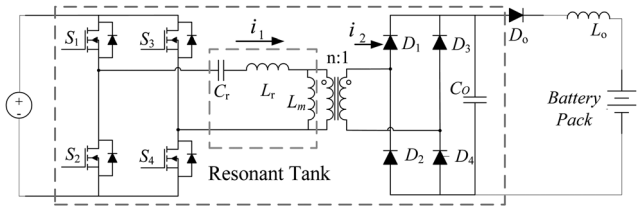

Fig. 1 *Schematic of a full bridge LLC converter*

doi: 10.1049/iet-est.2013.0016

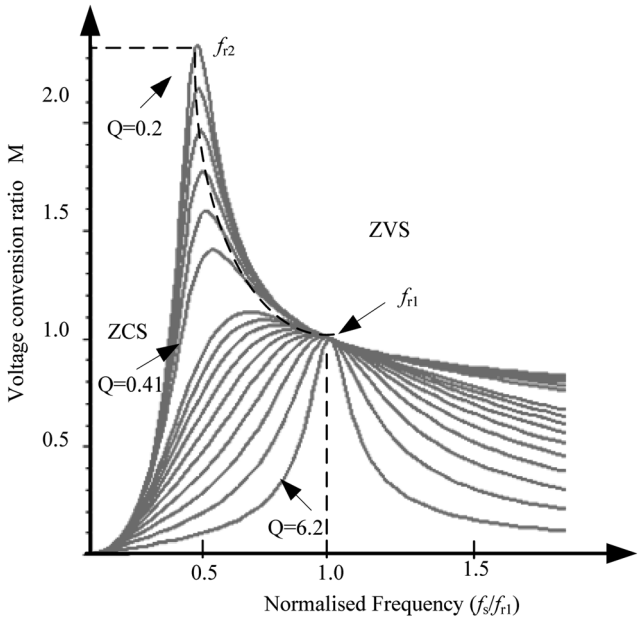

Fig. 2 *Frequency response of the output voltage under load variations*

and ZCS methods can be achieved in a LLC converter for different applications. For power MOSFET, ZVS is preferred because ZCS results in current spike during turn on transient leading to high-current stress and high-switching loss [16]. Fig. 2 depicts the ZVS and ZCS regions in a LLC resonant converter. The converter has three operation modes in responding to the switch frequencies. In mode 1 ($f_s > f_{r1}$), the impendence of the resonant tank is inductive, the converter operates under ZVS condition. The converter works in buck mode. In mode 3 ($f_s < f_{r2}$), the impendence of the resonant tank is capacitive, so the converter operates under ZCS condition. Mode 2 ($f_{r2} < f_s < f_{r1}$) is multi-resonant converter mode. The load situation determines the converter operation under ZVS or ZCS conditions. In both regions 2 and 3, the converter works in boost mode.

Based on the analysis above, we can see that for the design of LLC converters applied to on-board battery chargers, both the soft switching and the impact of battery load properties should be considered to ensure high performance and efficiency.

3 Design of switching frequency range

As mentioned in Section 1, different from a PWM converter, the switch current in a resonant converter is equal to the resonant tank current i_1 and is less dependent on load current. The tank current is determined by the tank input impedance Z_{in} ($j\omega_s$) that can be expressed as

$$Z_{in}(j\omega_s) = \frac{V_{s1}(j\omega_s)}{i_1(j\omega_s)} \tag{4}$$

The asymptotes of the magnitude of input impedance $||Z_{in}||$ in the open circuit and short circuit cases are illustrated in Fig. 3. The variation of $||Z_{in}||$, according to different load situations, is between the two limits. As the load increases, $||Z_{in}||$ curve

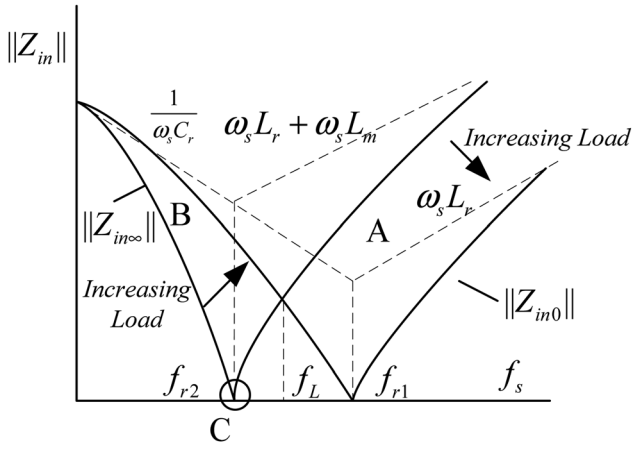

Fig. 3 *System input impedance with different load and switching frequency*

moves from $||Z_{in\infty}||$ to $||Z_{in0}||$ that is given by

$$Z_{i0} = Z_i|_{R_{Load}\to 0} = j\omega_s L_r + \frac{1}{j\omega_s C_r} \tag{5}$$

$$Z_{i\infty} = Z_i|_{R_{Load}\to \infty} = j\omega_s L_r + j\omega_s L_m + \frac{1}{j\omega_s C_r} \tag{6}$$

Fig. 3 depicts the behaviour of $||Z_{in}||$ for intermediate load value between the open-circuit and short-circuit conditions. In region A, $||Z_{in}||$ decreases as the load increases. In region B, $||Z_{in}||$ increases as the load increases. Consequently, the tank current in region B increases as the load decreases. Such a converter has a poor efficiency in the CV charging stage where the load current is small. Even if the load is reduced and removed, the system would approach point C in Fig. 3, resulting in the largest tank current. Thus, to improve light-load efficiency, $||Z_{in}||$ should increase as the load decreases, such as in region A. The switching frequency edge between region A and region B can be calculated as $||Z_{i0}||$ equals $||Z_{i\infty}||$. The switching frequency in the CV charging stage should be higher than the value of f_L

$$f_L = \frac{\sqrt{2}}{2\pi\sqrt{(2L_r + L_m)C_r}} \tag{7}$$

4 Impact of battery load roperty on the LLC resonant converter

As shown in Fig. 2, both ZCS and ZVS exist in the region $f_{r2} < f_s < f_{r1}$. In the previous literature, the design of the LLC resonant converter with ZVS focused on the selection of inductance L_m and L_r because $Z_{in}(j\omega_s)$ is dominated by the tank inductor [12]. The effect of the resonant capacitor C_r is often ignored.

In the PHEV charger application, however, the battery load has significant impacts on the converter through resonant capacitor C_r. An upper limit of capacitor voltage can be calculated as

$$V_{cr}^* = n\left(1 + \frac{L_r}{L_m}\right)V_{Load} + V_{in} \tag{8}$$

When the voltage across capacitor V_{cr} is lower than V^*_{Cr} in

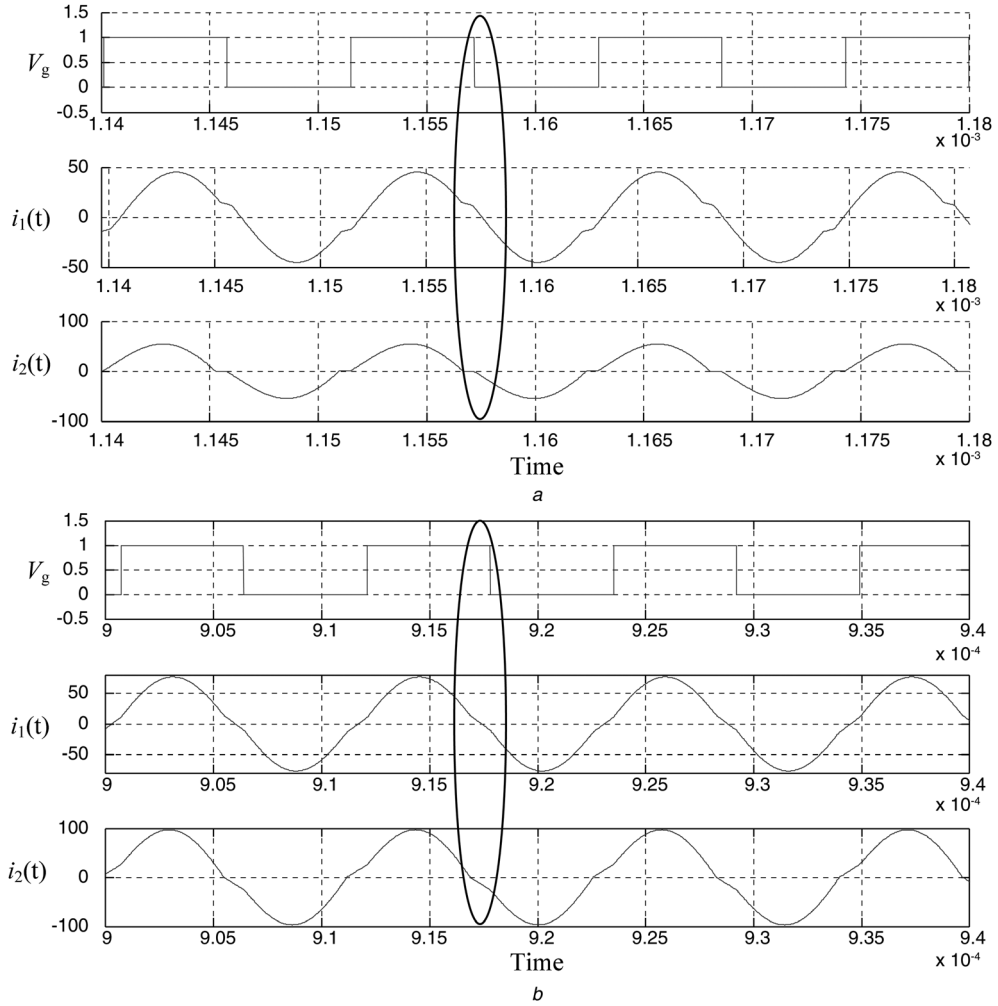

Fig. 4 *Comparison of the waveforms when converter works in*

a ZVS region
b ZCS region

(8), after the tank current i_1 resonates back to the level of L_m current, it would be clamped by the L_m current, as shown in Fig. 4*a*. The secondary-side diodes do not conduct during this period and the direction of the tank current would not change until switch devices turn on, allowing ZVS to be achieved. If the switching current keeps increasing and makes voltage V_{cr} on the resonant capacitor higher than V^*_{Cr} in (8), the energy stored in the capacitor could be high enough to make the secondary-side diode conduct, as shown in Fig. 4*b*. This can force the tank current to

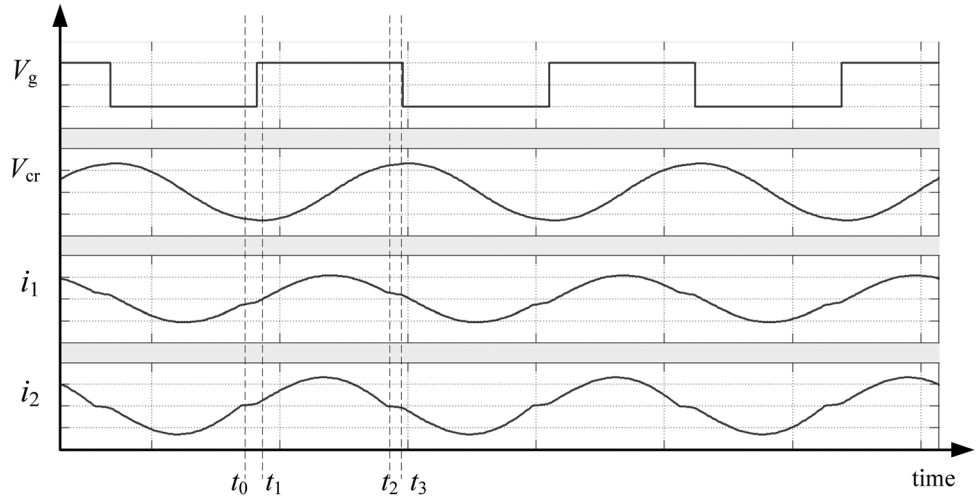

Fig. 5 *Simulation results when the system approaches the boundary between ZVS and ZCS*

doi: 10.1049/iet-est.2013.0016

resonate to the other direction [17]. If the tank current resonates to negative, current leads voltage V_{s1}.The converter operates in ZCS condition.

The influence of resonant capacitor C_r, however, is not significant with a passive load. When connected to a passive load, the load voltage V_{load} increases as the load current increases, allowing the upper limit V^*_{Cr} to increase. For the battery load, however, the load voltage, $V_{battery}$, is a relatively constant value. It is related to the SOC and is less dependent on load current. It can clamp the upper limit V^*_{Cr}, allowing V_{cr} to exceed V^*_{Cr} in a heavy load condition. Then the converter fails to achieve ZVS condition.

Hence, the passive load assumption is not suitable for the design of a PHEV battery charger. For the battery load consideration, the boundary between ZVS and ZCS with a CV load needs to be figured out. The waveform of current i_1, i_2 and voltage V_{cr} when the converter approaches that boundary is shown in Fig. 5.

In Fig. 5, during $[t_0 \sim t_2]$: at the time t_0, switch S_2 turns off, the resonant current flows through the body diode in S_1, voltage across S_1 decrease to zero. After a short interval from t_0, switch S_1 turns on with ZVS. The equation for the whole procedure can be written as:

$$\begin{cases} V_{in} - V_{cr} - nV_{load} = L_r \dfrac{di_1}{dt} \\ C_r \dfrac{dV_{cr}}{dt} = i_1 \\ L_m \dfrac{di_{L_m}}{dt} = nV_{load} \end{cases} \tag{9}$$

In Fig. 5, during $[t_0 \sim t_2]$: at time t_0, switch S_2 turns off, the resonant current flows through the body diode of S_1, and the initial conditions are $i_1(t_0) \simeq i_{L_m}(t_0) = I_{1t_0}$, $u_{cr}(t_0) = V_{cr0}$. We can obtain the solution as (see (10))

where $\omega_r = 1/\sqrt{L_r C_r}$. At time t_2, $i_1(t_2) = i_{Lm}(t_2) = I_{1t2}$, diodes D_1 and D_4 turn off. Current $i_2(t_2)$ in the secondary side is zero. Equation (10) describes the voltage and current waveforms in the capacitor during $[t_0 \sim t_2]$.

The initial value of current and voltage contained in (10) needs to be figured out. In Fig. 9, when the waveform in the ZVS/ZCS boundary: (1) The current value I_{1t0} at t_0 is close to zero; (2) the peak value of the voltage in resonant capacitor C_r is achieved near time t_0. According to that, (10) can be simplified as (see (11))

From (11) and (8), the critical V^*_{load} at the boundary between ZVS and ZCS can be derived as:

$$\begin{aligned} &(nV^*_{load} + V_{cr0} - V_{in})L_m \cos[\omega_r(t_2 - t_0)] \\ &\quad > nV^*_{load}(2 \cdot L_m + L_r) \end{aligned} \tag{12}$$

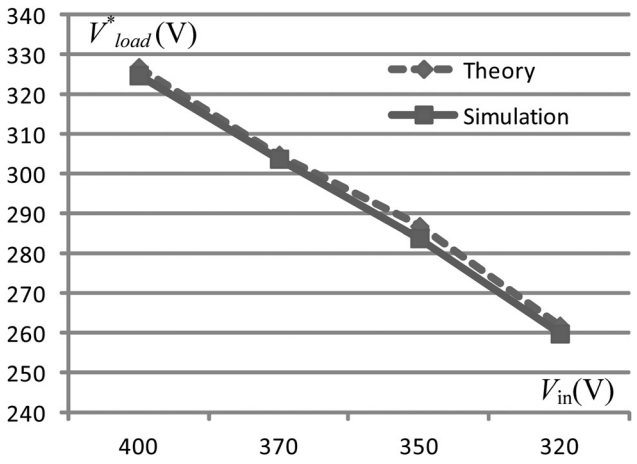

Fig. 6 *Verification of (13) under different input voltage*

$$V^*_{load} = \frac{(V_{cr0} - V_{in})L_m \cos\alpha}{(2L_m - L_m \cos\alpha + L_r)n} \tag{13}$$

where $\alpha = \omega_r(t_2 - t_0)$.

Equation (13) is verified under different input voltage V_{in} situations in Fig. 6. The solid line shows the value of V^*_{load} calculated by (13) with different V_{in} and the dashed line is the load voltage from simulation which can make the tank current resonate to negative at t_2. V^*_{load} in (13) matches well with the result from simulation.

Equation (13) illustrates that the critical load voltage at the ZVS/ZCS boundary is determined by the input voltage V_{in}, the resonant tank and V_{cr0}. Next, it is worth to estimate V_{cr0} in (13) for the simplification of optimal design. In Fig. 1, because of the output capacitor, the dc component of $|i_2(t)|$ must equal the steady-state output current I_{load}. Thus, we can obtain

$$I_{load} = \frac{2}{T_s}\int_0^{\frac{T_s}{2}} I_2 |\sin(\omega_s t - \varphi)| dt = \frac{\pi}{2} I_2 \tag{14}$$

From (11), we can obtain

$$V_{cr0} = V_{in} - nV_{load} - \frac{I_1}{C_r \omega_r} \tag{15}$$

From (13), (14) and (15), V_{cr0} can be eliminated and the relationship between I^*_{load}, V^*_{load} and resonant frequency ω_{r1} can be derived as

$$\omega_{r1} = -\frac{1}{2}\frac{L_m \cos(\alpha)\pi}{n^2 V^*_{load}(2L_m + L_r)C_r} I^*_{load} \quad \frac{\pi}{2} < \alpha < \pi \tag{16}$$

$$\begin{cases} V_{cr}(t) = (nV_{load} + V_{cr0} - V_{in})\cos[\omega_r(t - t_0)] + L_r \omega_r I_{1t0} \sin[\omega_r(t - t_0)] + V_{in} - nV_{load} \\ i_1(t) = I_{1t0}\cos[\omega_r(t - t_0)] + C_r \omega_r (V_{in} - nV_{load} - V_{cr0})\sin[\omega_r(t - t_0)] \\ i_{L_m}(t) = I_{1t0} + \dfrac{nV_{load}}{L_m}(t - t_0) \end{cases} \tag{10}$$

$$\begin{cases} U_{cr}(t) \simeq (nV_{load} + V_{cr0} - V_{in})\cos[\omega_r(t - t_0)] + V_{in} - nV_{load} \\ i_1(t) \simeq I_1 \sin[\omega_r(t - t_0)] = C_r \omega_r (V_{in} - nV_{load} - V_{cr0})\sin[\omega_r(t - t_0)] \end{cases} \tag{11}$$

Equation (16) represents the lowest resonant frequency ω_r to ensure ZVS with the desired load current I^*_{load} in V^*_{load}. For a LLC converter whose resonant frequency is ω_{r1} and if the charging current excesses I^*_{load} with load as V^*_{load}, ZVS would disappear. Let $\omega_{r1} = 1/\sqrt{L_r C_r}$, we can obtain the expression of resonant capacitor value as

$$C_r = \left(\frac{1}{2} \frac{\sqrt{L_r} L_m \cos(\alpha)\pi}{n^2 V^*_{load}(2L_m + L_r)} I^*_{load} \right)^2 \quad (17)$$

The resonant capacitor value should be larger than the value calculated in (17) to ensure ZVS with given I^*_{load} in V^*_{load}. The characteristic of the LLC converter at boundary condition between ZVS and ZCS in the CC charging stage has been derived. Next, it is instructive to consider the maximum current I_{outmax} the LLC converter can output at the boundary. Only if I_{outmax} turns to be larger than I^*_{load}, the whole system can output I^*_{load} and V^*_{load} with a battery load in the ZVS condition. From (10), we can obtain the transformer secondary-side current

$$i_2(t) = i_{cr}(t) - i_{L_m}(t) \quad (18)$$

Take the derivative of (18) with respect to t, the peak value of $i_2(t)$ can be derived when the derivative is set to zero at time t_{1a}

$$\frac{d(i_{cr} - i_{L_m})}{dt} = 0 \quad (19)$$

$$t_{1a} = cos^{-1}\left(\frac{nV^*_{load}}{\omega_r^2 C_r (V_{in} - nV^*_{load} - V_{cr0}) L_m} \right) \omega_r^{-1} + t_0 \quad (20)$$

From (18) and (20) and we can obtain the maximum value of $i_2(t)$

$$I_2 = \omega_r C_r (V_{in} - nV^*_{load} - V_{cr0}) \times \sqrt{1 - \frac{n^2 V^{*2}_{load}}{\omega_r^4 C_r^2 (V_{in} - nV^*_{load} - V_{cr0})^2 L_m^2}} - nV^*_{load} cos^{-1}\left(\frac{nV^*_{load}}{\omega_r^2 C_r (V_{in} - nV^*_{load} - V_{cr0}) L_m} \right) L_m^{-2} \omega_r^{-1} + I_{Lm0} \quad (21)$$

In (21), V_{cr0} can be estimated by (14) and (15) and I_{LM0} can be calculated from (10)

$$I_{Lm0} \simeq \frac{nV^*_{load}}{L_m} \frac{1}{4\omega_r} \quad (22)$$

From (21) and (15), we can obtain

$$I_{max} = \frac{\pi}{2} \left(\omega_r C_r (V_{in} - nV^*_{load} - V_{cr0}) \sqrt{1 - \frac{n^2 V^{*2}_{load}}{\omega_r^4 C_r^2 (V_{in} - nV^*_{load} - V_{cr0})^2 L_m^2}} - nV^*_{load} cos^{-1}\left(\frac{nV^*_{load}}{\omega_r^2 C_r (V_{in} - nV^*_{load} - V_{cr0}) L_m} \right) - L_m^{-1} \omega_r^{-1} + I_{Lm0} \right) \quad (23)$$

Equation (23) demonstrates the maximum current at the boundary between ZVS and ZCS with a given load voltage V^*_{load} in the CC charging stage.

5 Optimal design of LLC converter in a PHEV battery charger

Based on the analysis presented in the previous sections, the optimal design of LLC converter for the PHEV battery charger application is proposed in this section. First, for the CV charging stage, the minimum switching frequency needs to be calculated following (7).

In the first step, the system is designed following the normal design procedure in [3, 5, 14] with the system parameters. The value of L_m, L_r and C_r in the LLC resonant tank can be calculated. Then, the minimum switching frequency f_{min} can be calculated as f_L in (7). If M_{max} at the minimum switching frequency f_{min} is smaller than the desired value $M_1 = V_{outmax}/V_{outmin}$, then the design should go back to the first step to reselect the component values.

For the CC charging function, additional design steps are needed. The resonant frequency ω_{r1} is calculated from (16), according to the desired maximum output current I^*_{load}. Then, the minimum resonant capacitor C^*_r can be calculated in (17) and the maximum output current I_{max} can be estimated by (23). Only if I_{max} is higher than I^*_{load}, the system is capable to output the desired current I^*_{load} for the constant charging.

6 Simulation and experimental results

The aim of this section is to design a 6 kW LLC resonant dc–dc converter used in a PHEV on-board battery charger using the procedures proposed in the previous sections. The input voltage of the resonant dc–dc converter is 400 V. The output voltage range is from 330 to 500 V. According to

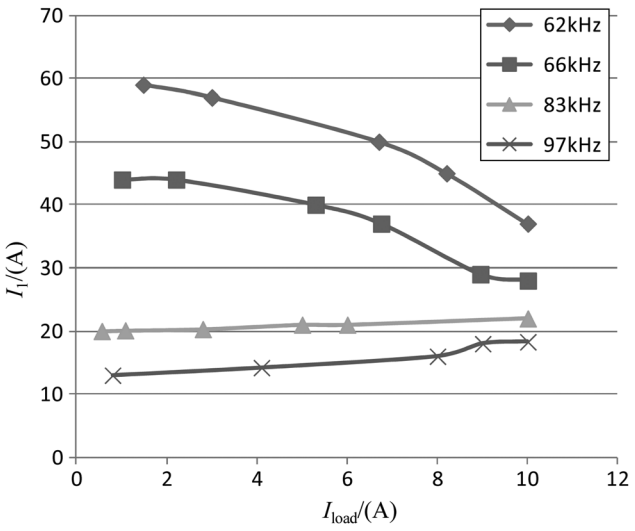

Fig. 7 *Load-dependent property under different switching frequencies*

doi: 10.1049/iet-est.2013.0016

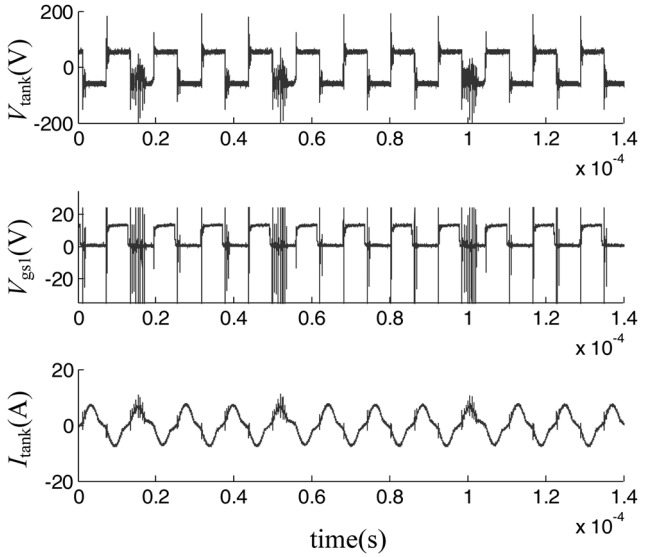

Fig. 8 *Battery load experiment with the failure of ZVS*

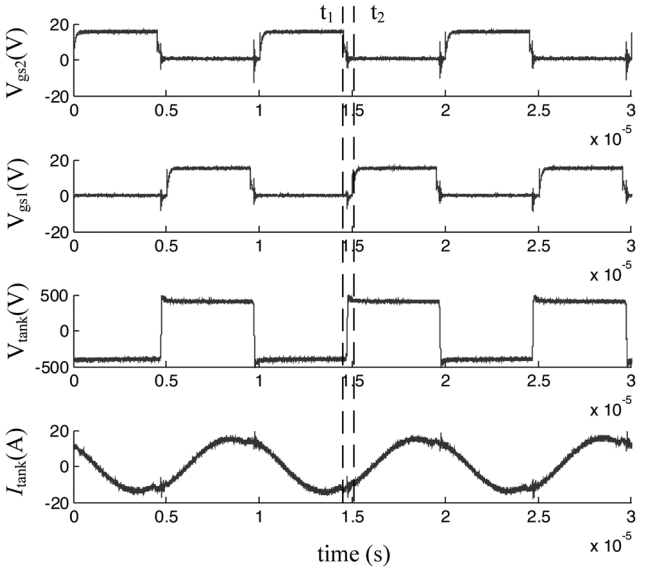

Fig. 10 *Battery load experiments with ZVS at V_{out} = 400 V, I_{out} = 10 A*

the optimal design proposed in Section 4, the values of the resonant tank components are selected as: $L_r = 40$ μH, $L_m = 80$ μH, $C_r = 68$ nF and the turn ratio value is 1.3. The two resonant frequencies are $f_{r1} = 97$ kHz, $f_{r2} = 55$ kHz, respectively. Frequency f_L is 68 kHz. Maximum operation frequency is 160 kHz. The system consists of following components: MOSFET(IPW60R045CP) and Diode (FFH60UP60S3).

Fig. 7 shows the profiles of I_1 and I_{load} under different switching frequencies. It can be seen that when $f_s > f_L$, I_1 would increase as I_{load} increase. when $f_s < f_L$, however, I_1 would increase as I_{load} decreases, resulting in poor efficiency in the CV charging stage. The simulation results agree with the analysis in Section 3.

To verify the analysis presented in Section 4, a lithium-ion battery pack rated at 400 V is utilised as the battery load for the charge experiments. The experiments are conducted in the region $f_L < f_s < f_{r1}$ with a battery load at load current of 3 A. Fig. 8 shows the current and voltage waveforms in the resonant tank when the system crosses the ZVS/ZCS boundary and enter ZCS region. It can be seen that the tank current resonates to negative before the device turns on. The failure of ZVS caused severe EMI in the switch signal V_g. The EMI issue would caused false triggering in devices resulting in short-circuit fault.

After improvement according to the procedures in Section 4, ZVS could be guaranteed in the whole output voltage range. Fig. 9 shows steady-state experiment at CC charge of 10 A with load voltages from 340 and 380 V. The input of LLC converter is provided by a PFC stage in the on-board charger that transfers 200 V ac voltage to 400 V dc voltage. It can be seen that the PFC current gets well controlled with LLC converter. The designed resonant tank in the on-board charger can output desired large current with ZVS in different load voltage situations.

Fig. 10 shows the tank current and voltage experiment waveforms operating at output voltage 400 V and output current 10 A with a battery load. At time t_1, the low side

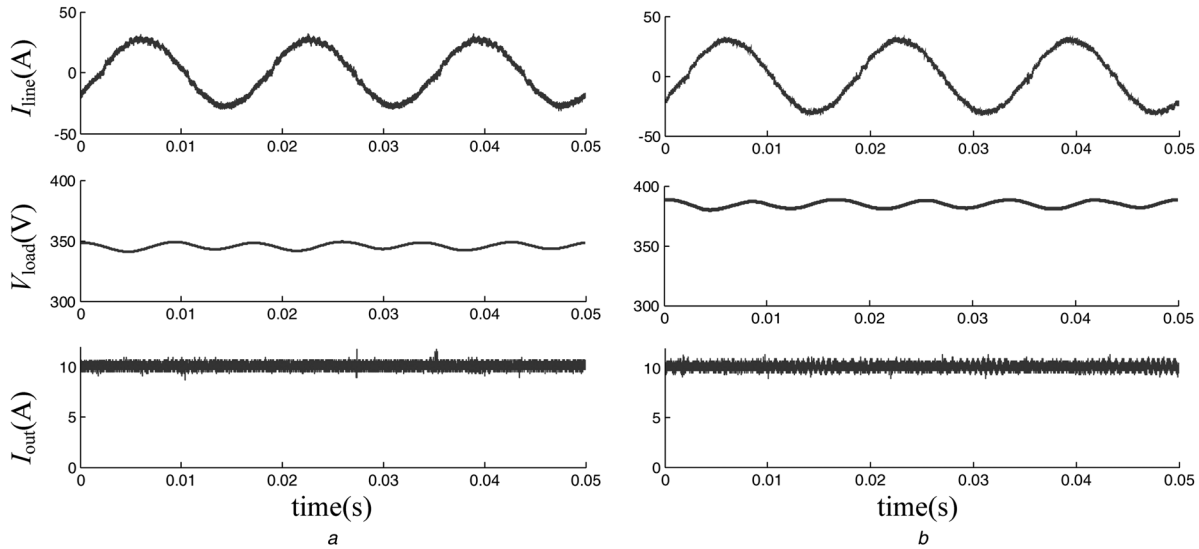

Fig. 9 *LLC steady-state test as an on-board charger with various battery load I_{load} = 10 A, V_{in} = 200 V*

a V_{load} = 340 V
b V_{load} = 380 V

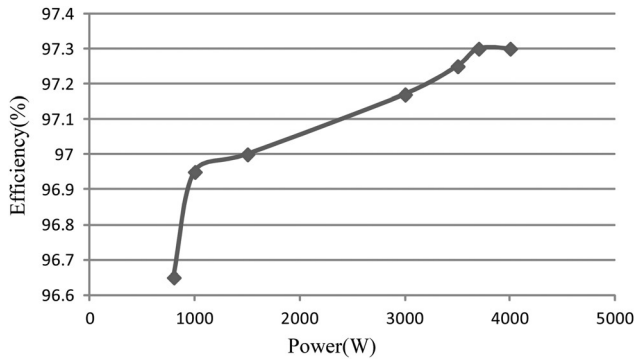

Fig. 11 *Efficiency of the LLC resonant converter with a battery load*

MOSFET S_2 is turned off by V_{gs2} and the tank current forces the upper diode in S_1 to conduct. So the tank voltage changes to positive in a short interval. When it reaches V_{dc}, the capacitor on S_1 is fully discharged. Then S_1 is turn on in ZVS by V_{gs1} at time t_2. Owing to ZVS, the EMI in switch signal V_g vanished and the efficiency is more than 97% as shown in Fig. 11.

7 Conclusions

This paper introduced the LLC resonant converter topology into PHEV battery chargers. For this purpose, the requirement and challenges for the LLC converter applied in battery charger systems have been discussed. The deficiency of previous LLC topology studies based on passive load assumption is investigated. Then the paper studied the optimal design method for the LLC converter applied in PHEV battery chargers in two approaches. First, to improve the efficiency in the light-load conditions during the CV charging stage, the optimum LLC switching frequency range is derived. Second, considering the CC charging function of PHEV battery chargers, the impact of battery load on the LLC converter was discussed. The characteristics of the LLC converter with a battery load at the boundary between ZVS and ZCS is analysed. A trade-off among the minimum load voltage, maximum charging current and resonant capacitance has been studied in detail. Finally, an optimal design method for the LLC resonant converter used in the PHEV battery charger for CV/CC charging is proposed. The proposed methods are validated through experiments on a 400 V/6 kW PHEV charger system with 97% efficiency.

8 References

1 Gautam, D., Musavi, F.: 'An automotive on-board 3.3 kW battery charger for PHEV application', *IEEE Trans. Veh. Technol.*, 2012, **61**, (8), pp. 3466–3474

2 Khaligh, A., Dusmez, S.: 'Comprehensive topological analysis of conductive and inductive charging solutions for PHEV', *IEEE Trans. Veh. Technol.*, 2012, **61**, (8), pp. 3475–3489

3 Liu, W., Liang, Y., Lee, F.C.: 'Optimal design methodology for LLC resonant converter'. Proc. IEEE Applied Power Electronic Conf. and Exposition, Dallas TX, March 2006, pp. 533–538

4 Choi, H.: 'Analysis and design of LLC resonant converter with integrated transformer'. Proc. IEEE Applied Power Electronic Conf. and Exposition, March 2007, pp. 1630–1635

5 Yang, B., Lee, F.C., Zhang, A.J., Huang, G.: 'LLC resonant converter for front end DC/DC conversion'. Proc. IEEE Applied Power Electronic Conf. and Exposition, Dallas, TX., March 2002, pp. 1108–1112

6 Beiranvand, R., Rashidia, B.: 'A design procedure for optimizing the LLC resonant converter as a wide output range voltage source', *IEEE Trans. Power Electron.*, 2012, **27**, (4), pp. 3749–3763

7 Beiranvand, R., Rashidia, B.: 'Optimizing the normalized dead-time and maximum switching frequency of a wide-adjustable-range LLC resonant converter', *IEEE Trans. Power Electron.*, 2011, **26**, (2), pp. 462–472

8 Hu, Z.Y., Qiu, Y.J.: 'An interleaved LLC resonant converter operating at constant switch frequency'. Proc. IEEE Energy Conversion Congress and Exposition, Raleigh, NC, September 2012, pp. 3541–3548

9 Tomokazu, M., Mizutani, H.: 'An LLC resonant full-bridge inverter-link DC-DC converter with an anti-resonant circuit for practical voltage step-up/down regulation'. Proc. IEEE Energy Conversion Congress Exposition, Raleigh, NC, September 2012, pp. 3533–3540

10 Musavi, F., Craciun, M., Gautam, D.S., Eberle, W., Dunford, W.G.: 'An LLC resonant DC-DC converter for wide output voltage range battery charging applications', *IEEE Trans. Power Electron.*, 2013, **28**, (12), pp. 5437–45

11 Musavi, F., Craciun, M., Edington, M., Eberle, W., Dunford, W.G.: 'Practical design considerations for a LLC multi-resonant DC-DC converter in battery charging applications'. Proc. IEEE Applied Power Electronic Conf. and Exposition, Orlando FL, February 2012, pp. 2596–2602

12 Dickinson, B., Gill, J.: 'Issues and benefits with fast charging industrial batteries'. Proc. 15th Annual Battery Conf. on Applications and Advancement, Long Beach, CA, January 2000, pp. 11–14

13 Li, S., Zhang, C., Xie, S.: 'Research on fast charge method for lead-acid electric vehicle batteries'. Proc. Int. Workshop on Intelligent Systems and Applications, Wu Han, China, May 2009, pp. 23–24

14 Oruganti, R., Lee, F.C.: 'Resonant power processors. II. Methods of control', *IEEE Trans. Ind. Appl.*, 1985, **21**, (6), pp. 1461–1471

15 Chang, C.C., Chang, E.: 'A high-efficiency solar array simulator implemented by an LLC resonant DC-DC converter', *IEEE Trans. Power Electron.*, 2013, **28**, (6), pp. 3039–3046

16 Erickson, R.W., Maksimovic, D.: '*Fundamentals of power electronics*' (Kluwer, Norwell, 2006), p. 722

17 Yang, B.: 'Topology investigation for front end DC-DC power conversion for distributed power system'. Ph.D. thesis, Department of Electronic Engineering, Virginia Polytechnic Institute and State University., September 2003

doi: 10.1049/iet-est.2013.0016